ORIGINAL PAPER

Solid-state dye-sensitized ZnO solar cells prepared by low-temperature methods

Yvonne Selk · Melanie Minnermann · Torsten Oekermann · Michael Wark · Jürgen Caro

Abstract Solid-state dye-sensitized solar cells based on highly porous ZnO films prepared by template-assisted electrodeposition as electron collector, the indoline dye D149 as sensitizer and CuSCN as hole collector have been prepared using three different methods, namely impregnation with saturated CuSCN solution, successive ionic layer adsorption and reaction (SILAR) and electrodeposition, for filling the pores in the ZnO with CuSCN. The highest pore filling and the highest conversion efficiency of 0.46% were achieved with the impregnation method, while SILAR led to a very low pore filling, causing very low photocurrents, and electrodeposition led to short-circuiting between the CuSCN and the conducting substrate of the ZnO sample despite the presence of a compact ZnO bottom layer between the porous ZnO layer and the conducting layer, causing very low open-circuit voltages.

Keywords Dye-sensitized solar cells · Electrodeposition · Zinc oxide · Copper thiocyanate

1 Introduction

Cathodic electrodeposition of ZnO in the presence of structure-directing additives is a valuable new route for the

Y. Selk · M. Minnermann · T. Oekermann (✉) ·
M. Wark · J. Caro
Institute of Physical Chemistry and Electrochemistry,
Leibniz Universität Hannover, Callinstrasse 3-3A,
30167 Hannover, Germany
e-mail: torsten.oekermann@pci.uni-hannover.de

Present Address:
T. Oekermann
Friemann & Wolf Batterietechnik GmbH, Industriestraße 22,
63654 Büdingen, Germany

preparation of nanoporous wide band gap semiconductor films for dye-sensitized solar cells (DSSC) [1]. The main advantage of the method is that fully crystalline material is directly obtained during the electrodeposition process without the need for further heat treatment [2]. Dye molecules with acid groups, which can interact with Zn^{2+} and are therefore incorporated into the growing ZnO film, were among the first structure-directing agents used in this method [3, 4]. While the original goal to deposit efficient dye-sensitized ZnO films in a single step could not be achieved due to dye aggregation occurring during the deposition, the dye aggregates proved to be ideal templates for the low-temperature preparation of porous ZnO films, since they can easily be extracted from the as-deposited ZnO/dye hybrid films by treatment with aqueous KOH. The same or another dye can then be re-adsorbed to the films to obtain a dye-monolayer for efficient sensitization [5].

ZnO films with an especially high porosity were obtained by deposition from solutions containing O_2 as oxidant and the xanthene dye eosin Y (EY) as structure-directing additive [5, 6]. After EY desorption and loading with the indoline dyes D149 [7] and DN98 [8], respectively, these films were successfully tested in dye-sensitized solar cells, reaching efficiencies of 5.6 and 6.24%, which are among the highest efficiencies for DSSC prepared by a low-temperature method to date (including low-temperature films of TiO_2). The values are also higher than efficiencies obtained with high-temperature films made from ZnO nanoparticles. This is due to the excellent electron transport properties of the electrodeposited ZnO films, which was attributed to the virtual absence of grain boundaries in these films, which were found to consist of large porous single crystals [9]. An even better electron transport is expected and has also

been found for ZnO nanorods [10]. Nevertheless, the efficiencies achieved with ZnO nanorods were much lower, i.e., only 1.5% [11]. This is due to the inherently lower surface area of a film consisting of 1D nanostructures compared to a 3D nanostructure, given a comparable thicknesses of the films and the ZnO walls. It further contributes to the lower surface areas of the nanorod arrays used in these studies that the ZnO nanorods had diameters of at least 30 nm [11], compared to a wall thickness of down to ca. 10 nm for the ZnO films electrodeposited with EY as structure director.

A currently important topic concerning DSSC is the replacement of the liquid redox electrolyte, which facilitates the electron transport from the counter electrode to the photooxidized sensitizer dye molecules, by a solid or quasi-solid material, since the long-term prevention of liquid electrolyte leakage is still not fully solved. Many kinds of materials have been suggested for this purpose, e.g., gel electrolytes [12–16], polymer electrolytes [17–23], ionic polymers [24], molecular organic hole conductors [25], polymer hole conductors [22, 26–30] or the p-type semiconductors CuI [31, 32], CuSCN [31, 33–37], and NiO [38]. The filling of the pores in a dye-sensitized n-type semiconductor film with such materials is certainly easier when they consist of 1D structures such as nanorods. On the other hand, efficiencies reported for solid-state DSSC based on ZnO nanorods of 0.1% are even lower than for the nanorod-based cells with liquid electrolyte [39]. It is therefore clearly desirable to use 3D porous structures with a high surface area also for solid-state DSSC.

In this study the authors present first results on the use of the highly porous electrodeposited ZnO films templated with EY in solid-state DSSC based on a p-type semiconductor as hole collector. CuSCN has been chosen as the p-type material, since it can be deposited by various methods such as electrodeposition [40, 41], successive ionic layer adsorption and reaction (SILAR) [42, 43] and impregnation with a saturated CuSCN solution [34, 36, 44]. Furthermore, it has some advantages compared to NiO, which is poisonous and has shown low open-circuit voltages in TiO$_2$-based solid-state DSSC, and CuI, which initially leads to quite high efficiencies in TiO$_2$-based DSSC but has a poor long-term stability due to photooxidation of Cu(I) to Cu(II), while the Cu(I) in CuSCN is stable during illumination [31, 45]. DSSC have been prepared using D149 as sensitizer dye and CuSCN deposited by the three methods mentioned above. In addition, the pore filling achieved with these methods under various deposition parameters has been investigated in detail by scanning electron microscopy (SEM) in conjunction with energy-dispersive X-ray spectroscopy (EDXS).

2 Materials and methods

2.1 Preparation of porous dye-sensitized ZnO films

Porous ZnO substrates were electrodeposited at 70 °C from O$_2$-saturated aqueous ZnCl$_2$ solution (5 mM) containing 0.1 M KCl and 30 μM EY on glass covered with FTO (F-doped tin oxide, A.I. Glass, 10 Ω/sq) in a three electrode setup with a Zn wire as counter electrode and an Ag/AgCl electrode as reference electrode [7]. The deposition process consisted of three steps: (1) Pre-electrolysis without ZnCl$_2$ and EY at −1.1 V versus Ag/AgCl for 10 min, (2) deposition of a compact ZnO layer at −1.1 V versus Ag/AgCl for 10 min after addition of ZnCl$_2$ and (3) deposition of a ZnO/EY layer at −1.1 V versus Ag/AgCl for 20 min after addition of EY to the electrodeposition bath. The ZnO/EY layer was converted into a porous ZnO layer by extraction of the EY by aqueous KOH (pH 10.5) for 24 h. The FTO substrates were rinsed with acetone, ethanol, and isopropanol, for 30 min each, and attached to a rotating disc electrode (RDE, 300 rpm) with an active electrode area of 3.8 cm^2 in order to achieve a homogeneous film deposition. For dye sensitization, the substrates with the porous ZnO layers (Fig. 1) were dried at 120 °C for 1 h and immediately immersed into a solution containing 0.5 mM D149 dye and 1 mM cholic acid as co-adsorbant, which suppresses dye aggregation on the ZnO surface, in a mixture of acetonitrile and *tert*-butanol (1:1 by volume) for 30 min.
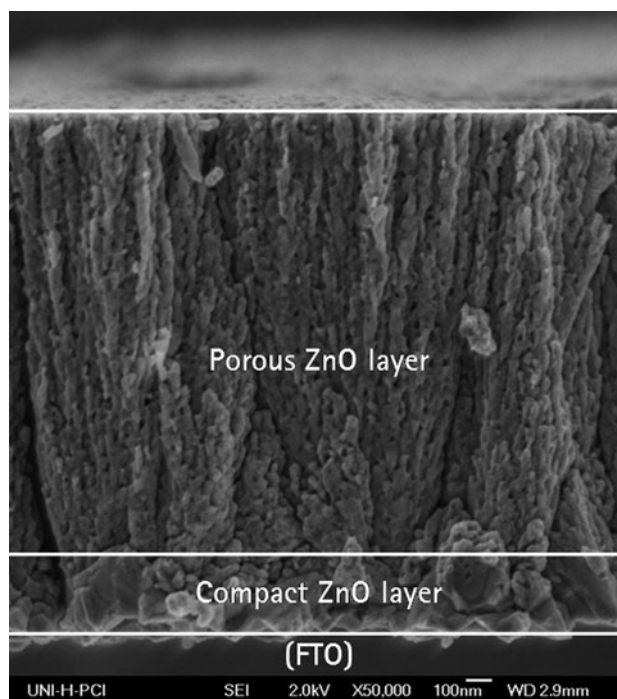
Fig. 1 SEM image of the cross section of a porous ZnO film with compact ZnO bottom layer after desorption of the EY template

2.2 Impregnation with CuSCN solution

Saturated solutions of CuSCN were obtained by stirring a mixture of 0.7 g CuSCN and 15 mL dipropylsulfide (DPS) over night and aging for 1 day. Impregnation of the dye-sensitized ZnO layers with this solution was carried out in three different ways: (1) Placing the ZnO substrates into a petri dish on a hotplate containing the CuSCN solution under variation of the solution level above the substrate, (2) dropwise addition of CuSCN solution onto a ZnO substrate directly located on a hotplate under variation of the volume of each drop and the number of drops added to the film and (3) dip-coating of a porous ZnO film into a CuSCN solution (50 times for 30 s, respectively, each step followed by 120 s drying at 80 °C).

2.3 CuSCN deposition by successive ionic layer adsorption and reaction (SILAR)

Following a method of Sankapal et al. [43] aqueous solutions of $CuSO_4$ (0.1 M) + $Na_2S_2O_3$ (0.1 M) and KSCN (0.1 M) were used as cation and anion sources. In one cycle, the ZnO films were first immersed into the anion source for 10 s, followed by washing in ultrapure water for 5 s, immersion into the cation source for 20 s and a final 5 s washing step. This cycle was repeated up to 50 times at room temperature.

2.4 Electrodeposition of CuSCN

CuSCN was electrodeposited on porous ZnO substrates from an aqueous solution containing 0.05 M KSCN, 0.01 M $CuSO_4$, and 0.1 M Triethanolamin (TEA) in a three-electrode setup with a Pt wire as counter electrode and an Ag/AgCl reference at 0 °C. Two different methods were used: (1) Deposition at a constant potential of −0.5 V versus Ag/AgCl for 1 h according to Ni et al.[41] and (2) deposition at +0.1 V versus Ag/AgCl for 10 min in order to promote nucleation and crystal growth, followed by a potential ramp (-1 mV s^{-1}) and deposition at −0.5 V versus Ag/AgCl for 40 min according to Wu et al. [40].

2.5 Preparation and measurement of solar cells

Gold layers were evaporated in vacuum on the deposited CuSCN layers using an Edwards vacuum deposition chamber. The gold layers and the FTO layers were contacted with copper wires using silver paste. $i–v$ curves of the prepared cells were measured with a Zahner IME 6e electrochemical workstation under illumination with simulated AM 1.5 sun light (Oriel 300 W Xe lamp + Oriel AM 1.5 filter).

2.6 Other characterization methods

The sensitizer dye contents in the porous ZnO was determined by dissolving a part of the films in N,N-dimethyl-acetamide (DMA), followed by measuring the UV/VIS absorption of the resulting solution with a Cary 4000 spectrometer. Film thicknesses were measured with a Dektak 6 M Stylus profiler. The nanostructure of the ZnO films before and after CuSCN deposition was studied using a field emission scanning electron microscope (SEM, Jeol JSM-6700). Cross section samples for SEM were prepared by pasting on a Si wafer, cutting with a wire saw and polishing with polymer-embedded diamond. For qualitative and semi-quantitative analysis of the elements contained in the different layers of the samples, the SEM was equipped with energy-dispersive x-ray spectroscopy (EDXS, Oxford Instruments INCA 300).

3 Results and discussion

3.1 Preparation of porous dye-sensitized ZnO films

Figure 1 shows the cross section of a typical sample with a compact and a porous ZnO film on FTO-covered glass. The compact layer has a thickness of only about 200–300 nm, reducing the impact of this layer on the series resistance of the solar cell compared to earlier studies with the same kind of porous ZnO sample, where the thickness of the compact ZnO layer was about 1 μm [7]. The porous ZnO layer has a thickness of about 1.5 μm, the porous structure consisting of twisted and interconnected nanowires [7] being clearly visible. Note that thicker porous films can be obtained by using longer deposition times for the porous layer, which was, however, not applied in this study in order to reduce the time for preparing the samples.

Figure 2 shows typical $i–t$ curve recorded during the deposition of a porous ZnO substrate. Pre-electrolysis in O_2-saturated aqueous KCl solution leads to a constant current after about 6 min, showing that the activation process has been completed (section a). Addition of $ZnCl_2$ (b) leads to a reduction of the cathodic current due to the formation of ZnO (section c). Within section c, an increase of the cathodic current is seen at the beginning of the deposition process, followed by decease to a constant level after a maximum has been reached. This behavior has often been seen for the deposition of compact ZnO films and is explained by Volmer-Weber growth (island growth), where the increase of the deposition current in the beginning can be attributed to the increasing surface of the initially formed seed crystals (3D growth phase), while the decrease of the current after the maximum indicates the merging of these crystals (transition from 3D to 1D growth) [46]. After
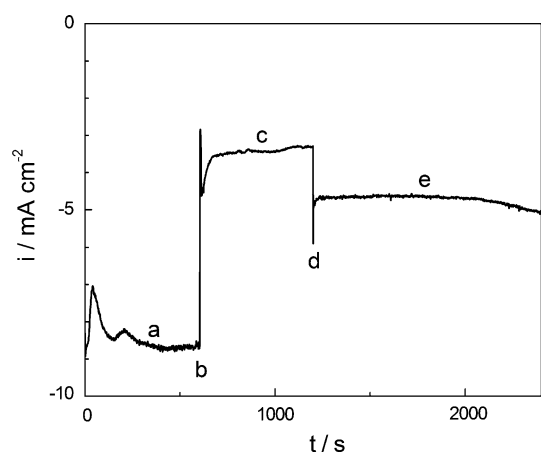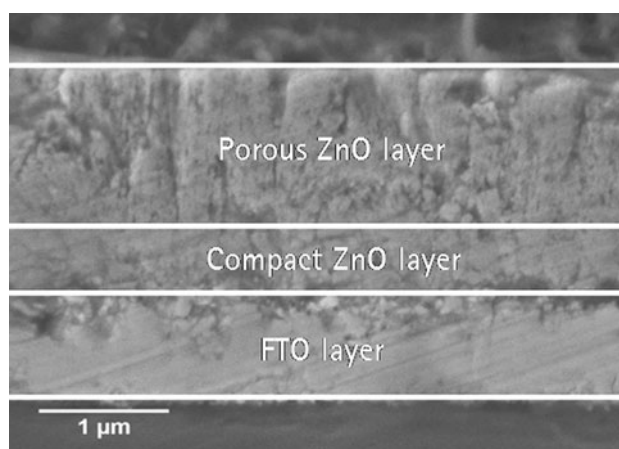
Fig. 2 Typical *i–t* curve recorded during the deposition of a porous ZnO substrate showing the following steps: **a** pre-electrolysis in O$_2$-satured aqueous KCl solution, **b** addition of ZnCl$_2$, **c** formation of the compact ZnO bottom layer, **d** addition of EY, **e** formation of the ZnO/EY layer, which is later turned into a porous ZnO layer by desorption of the EY

Fig. 3 Cross section SEM micrograph of a porous and compact ZnO layers (*top*) on an FTO layer (*bottom*) after impregnation with CuSCN solution

addition of EY (d), the cathodic deposition current increases significantly due to the catalytic effect of EY on the O$_2$ reduction [6] (section e). In this section, the current remains about constant, indicating 1D growth throughout the deposition of the ZnO/EY layer. The slight increase of the current towards the end of the deposition is explained by the increasing porosity and thereby increasing surface of the ZnO [47].

3.2 Impregnation with CuSCN solution

The three methods mentioned in the "Materials and methods" for the impregnation of ZnO substrates with CuSCN solution led to much different results. Immersion into CuSCN solution in a petri dish led to the formation of a rather thick (ca. 20 μm in average) but inhomogeneous CuSCN layer. On the other hand, reduction of the level of the solution above the ZnO sample led to the formation of a non-compact layer. A thin compact CuSCN layer could not be obtained. Since a thick compact CuSCN layer would lead to a high series resistance of the solar cell [34] and a non-compact CuSCN layer would give rise to short-circuiting between an evaporated contact layer and the ZnO, these samples were not investigated further. Similar results were also obtained by the dip-coating method.

Dropwise addition of CuSCN solution to the ZnO sample on a hotplate led to much better results. Firstly, this method resulted in the formation of much thinner (ca. 5 μm) yet homogeneous and compact CuSCN layers on top of the porous ZnO layer. Secondly, significant amounts of CuSCN were also deposited inside the porous ZnO layers. This is evident from the cross section SEM micrograph shown in Fig. 3 and the related EDXS results

shown in Fig. 4. In Fig. 3, it appears hard to distinguish between the porous and the compact ZnO layer above the FTO layer, which appears near the bottom of the micrograph (directly at the bottom a part of the glass is visible). This indicates that the pores in the porous ZnO layer have at least partly been filled by CuSCN. Consequently, in the EDXS mapping in Fig. 4 the porous ZnO layer can be identified by its higher sulfur content compared to other layers. The good pore filling is due to stepwise addition of impregnation solution leading to successive growth of CuSCN in the pores as well as upon the ZnO layer. This reduces the risk of pore blocking by CuSCN growing on top of the film.

A quantitative analysis of the sulfur content in the whole ZnO layer by EDXS gave a value of 0.45 atomic %. A slightly higher value of 0.55 atomic % was found for copper. In comparison, zinc was found with a content of 9.5 atomic %. Based on the densities of ZnO (5.61 g/cm^3) and CuSCN (2.85 g/cm^3) and assuming that about 2/3 of the ZnO layer is porous with a porosity (fraction of film volume not occupied by ZnO) of about 50% [7], it can be estimated that about 30% of the pore volume has been filled with CuSCN.

### 3.3 CuSCN deposition by successive ionic layer adsorption and reaction (SILAR)

In the SILAR method, cations and anions are deposited alternatingly on a surface, with excess ions washed away in between to assure layer-by-layer deposition occuring on the atomic level. Furthermore, the film thickness can be easily fine-tuned by the number of cycles, which determines the number of atomic layers [42]. This should make SILAR a suitable method for the filling of pores with CuSCN. However, Sankapal et al. [43] only reported the

Fig. 4 EDXS mapping for Sn, Zn, and S of the sample shown in Fig. 3. The division of the sample into porous ZnO layer, compact ZnO layer and FTO layer is indicated according to the mapping of the three elements
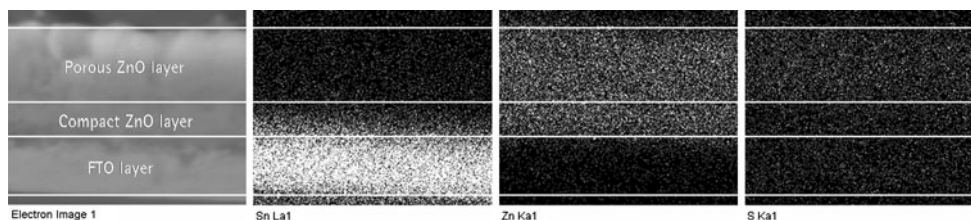
Fig. 5 EDXS mapping for Zn, Cu, and S of a porous ZnO sample after deposition of CuSCN by SILAR. The lines clarify the positions of the CuSCN (*top*), ZnO (*middle*) and FTO (*bottom*) layers
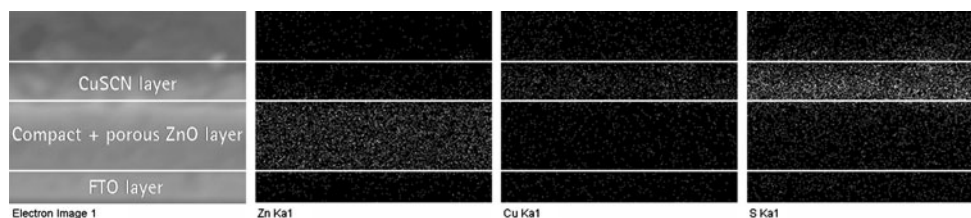
deposition of CuSCN films by SILAR on non-porous conducting glass substrates for applications in solar cells [43]. The authors found that it is not possible to deposit significant amounts of CuSCN into porous ZnO films, at least those with rather small pore sizes (<20 nm) as used in this study. This is demonstrated in the EDXS mapping of a porous ZnO substrate after deposition of CuSCN by SILAR in Fig. 5. It shows a compact CuSCN layer deposited above the porous ZnO layer, however, virtually no CuSCN deposited within the porous ZnO layer, considering that the signals are not more intense as for the FTO layer and therefore probably caused by the replacement of a small amount of CuSCN to these layers during the sample preparation for SEM.

A possible reason for the poor pore filling compared to impregnation might be that by loading one ion species at a time into the quite narrow pores of the ZnO network a partial charging of the pores occurs, leading to an electrostatic repulsion of further ions of the same charge. This inhibits the formation of a dense layer. Because the introduced ions relatively weakly interact with the non-charged ZnO network, the washing steps done in a SILAR cycle before the counter ion is introduced may lead to a further reduction of their surface coverage. The same effect is known from Si-rich zeolites, which can hardly be loaded with metal ions, unless a strong binding of cations in the pores is promoted by the incorporation of negatively charged AlO_2^- units into the SiO_2 framework.

On the rough external surface of the ZnO film the introduced charges can be better distributed than in narrow pores and thus the ion adhesion is improved. This leads to better growth of CuSCN than in the pores. The CuSCN grown on top of the ZnO layer eventually starts to block the pore entrances, and consequently the introduction of ions into the ZnO pore system is becoming increasingly difficult. By impregnation, in contrast, electroneutral CuSCN units are directly introduced into the ZnO pores and, thus, there is no repulsion effect in the pores and no preferential deposition on the external surface.

3.4 Electrodeposition of CuSCN

Electrodeposition of CuSCN into nanostructured ZnO layers for dye-sensitized solar cells has first been performed by O'Regan et al. [37] using an organic deposition solution. However, the use of organic solvents such as ethanol has some disadvantages, such as a lower conductivity compared to aqueous solutions, and possibly the partial desorption of the sensitizer dye [48]. The authors have therefore chosen two recently developed methods using aqueous solutions containing KSCN and $CuSO_4$ [40, 41] for the electrodeposition of CuSCN in this study.

Figure 6 shows the *i–v* curves for the CuSCN deposition in porous ZnO substrates according to both methods, i.e., the deposition at constant potential (Fig. 6a) and the three-step deposition including a potential ramp (Fig. 6b). Figure 6a shows a steep decrease of the deposition current immediately after the start of the deposition process. This decrease appears too large to be explained by a transition from 3D to 1D growth as in the electrodeposition of ZnO. Rather it seems to reflect the increasing resistance of a compact CuSCN layer deposited on top of the porous ZnO substrate. A top view of this compact CuSCN layer is seen in Fig. 7, revealing the typical large CuSCN crystals with sizes of hundreds of nm. When the three-step method is used (Fig. 6b), CuSCN deposition slowly starts during the potential ramp from +0.1 to −0.5 V versus Ag/AgCl at about −0.3 V versus Ag/AgCl. However, when the final potential of −0.5 V versus Ag/AgCl is reached, the further current transient behavior is very similar to that in Fig. 6a. The maximum current density reached at the end of the potential ramp in Fig. 6b is even lower than the initial
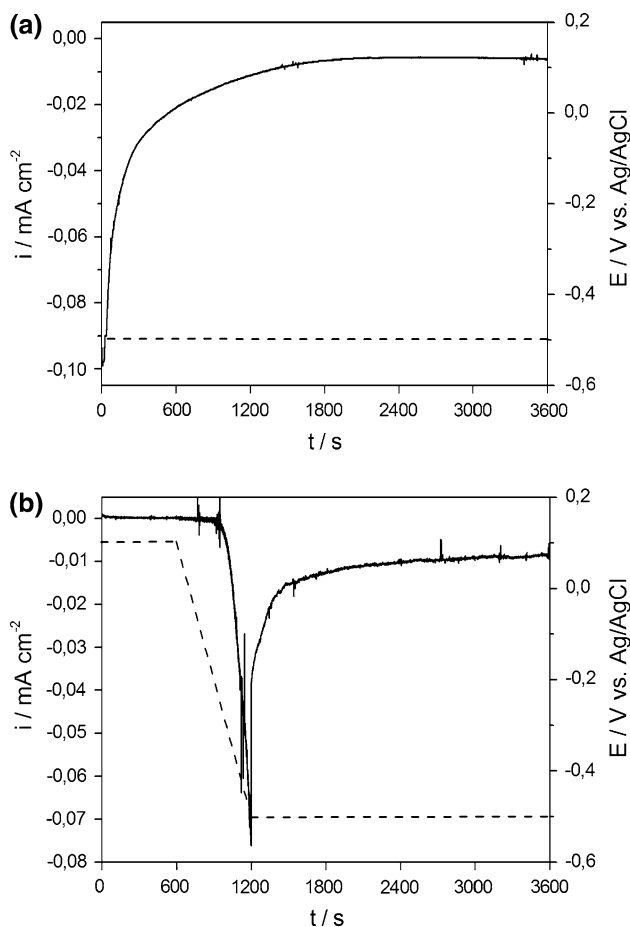
Fig. 6 i–v–t curves of the electrodeposition of CuSCN in porous ZnO substrates **a** at constant potential and **b** in a three-step process under variation of the deposition potential as indicated
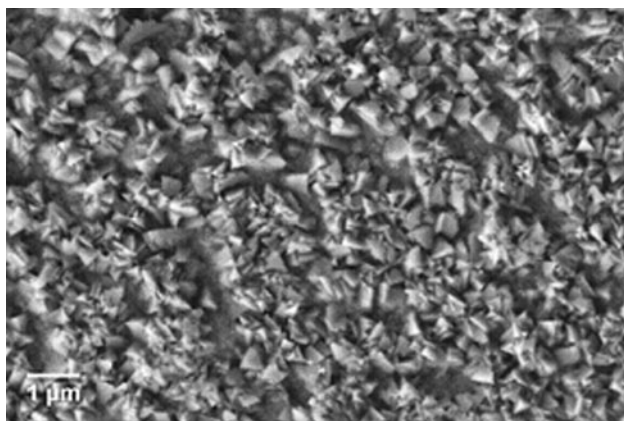
Fig. 7 SEM micrograph of an electrodeposited CuSCN layer deposited on a porous ZnO substrate at a constant potential of −0.5 V versus Ag/AgCl

Table 1 Zn and S contents from EDXS measurements for porous ZnO films after electrodeposition of CuSCN into the films using two different methods

Electrodeposition method	Zn content/ atom %	S content/ atom %	S/Zn ratio
Constant potential	18	0.46	0.026
Three-step method	15	0.06	0.004

capacitive, which is seen in the sudden drop of the current by about 50% immediately after the end of the ramp.

While EDXS mapping of the whole cross-sections of a porous ZnO substrates after CuSCN electrodeposition did not lead to explicit results concerning the CuSCN content of the ZnO layers, EDXS measurements at smaller sections of the ZnO layers led to some quantitative data, which are summarized in Table 1. By far the higher CuSCN content is achieved with electrodeposition at constant potential, although the content is only about half that achieved by impregnation for which a S/Zn ratio of 0.048 was found. The very low CuSCN content of the porous ZnO layer after applying the three-step method is rather surprising at first sight, since the potential ramp should actually enable the formation of more seed crystals due to the higher reactant concentration preserved in the pores due to the lower initial current density. However, it may be the case that the application of a potential ramp leads to the formation of seed crystals mainly where the electrolyte is in direct contact with the conducting FTO layer, e.g., where small cracks are present in the compact ZnO layer, and much less in the porous ZnO layer, because the electron concentration in this layer is too low before and at the beginning of the potential ramp.

Fig. 8 i–v curve of a ZnO/D149/CuSCN solar cell with CuSCN deposited into the porous dye-sensitized ZnO layer by impregnation under illumination with AM1.5 simulated sun light
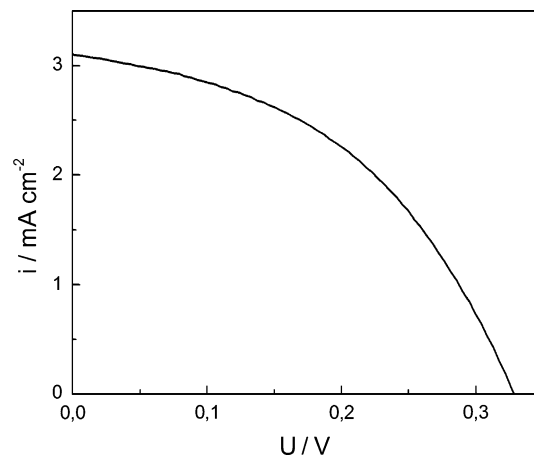
current density in Fig. 6a, so that an advantage of the three-step method is not evident. Furthermore, the current observed during the potential ramp seems to be partly

Table 2 Performance of the best ZnO/D149/CuSCN solar cells, respectively, with CuSCN deposited into the porous dye-sensitized ZnO layers by three different methods under illumination with AM1.5 simulated sun light

CuSCN deposition method	U_{oc}/mV	I_{sc}/mA cm^{-2}	FF	η/%
SILAR	215	0.16	0.32	0.011
Impregnation	330	3.1	0.45	0.46
Electrodeposition (constant potential)	41	1.52	0.28	0.017

3.5 Measurement of solar cell efficiencies

The performance of the best cells prepared using the three different deposition methods for CuSCN, respectively, are shown in Table 2. As expected from the highest CuSCN content in the porous ZnO film, the cell prepared by CuSCN impregnation shows the highest photocurrent and also the highest open-circuit voltage, leading an overall efficiency of 0.46% (*i–v* curve see Fig. 8). This is lower than the 1.5% achieved by O′Regan et al. [37] with a solid-state dye-sensitized solar cell based on ZnO and CuSCN, however, it has to be considered that, in opposition to the work of O′Regan et al., in this study all preparation steps have been carried out at low temperature suitable for flexible solid-state DSSC.

The solar cell prepared by SILAR shows a much lower photocurrent, which is expected from the very small amount of CuSCN deposited in the porous ZnO layer. Also the photocurrent observed with the cell prepared by CuSCN electrodeposition, which is about half that of the cell prepared by impregnation, is consistent with the amount of CuSCN deposited into the porous ZnO layer, since the S/Zn ratio for electrodeposition at constant potential was found to be about half that of the S/Zn ratio found for the impregnation method (see foregoing sub-chapter). It is striking, however, that the open-circuit voltage of the cell prepared by electrodeposition is very low compared to both other cells. This indicates that not only in case of the three-step electrodeposition method, but also in case of the CuSCN electrodeposition at constant potential some CuSCN is deposited directly from the conducting FTO layer, eventually leading to some short-circuiting.

4 Conclusions

The results of this study show that highly porous ZnO films prepared by template-assisted electrodeposition are in principle suitable for the preparation of solid-state dye-sensitized solar cells using CuSCN as hole conductor. The highest pore filling and efficiency was obtained with cells prepared by the impregnation of dye-sensitized porous ZnO films with saturated solutions of CuSCN in dipropylsulfide, which showed an efficiency of up to 0.46% despite a pore filling of only about 30% and the low ZnO layer thickness used in this preliminary study. Improvement of the pore filling and the use of thicker ZnO films should make possible an increase in efficiency by about one order of magnitude.

References

1. Yoshida T, Minoura H (2000) Adv Mater 12:1219
2. Peulon S, Lincot D (1996) Adv Mater 8:166
3. Yoshida T, Miyamoto K, Hibi N et al (1998) Chem Lett p 599
4. Yoshida T, Terada K, Schlettwein D et al (2000) Adv Mater 12:1214
5. Yoshida T, Iwaya M, Ando H et al (2004) Chem Commun p 400
6. Yoshida T, Pauporté T, Lincot D et al (2003) J Electrochem Soc 150:C608
7. Yoshida T, Zhang J, Komatsu D et al (2009) Adv Funct Mater 19:17
8. Yoshida T, Funabiki K, Matsui M et al (2009) Plastic solar cells employing electrodeposited zno and organic dye, 3rd International conference on the industrialization of DSC (DSC-IC), Nara, Japan, 22–24 Apr 2009
9. Oekermann T, Yoshida T, Minoura H et al (2004) J Phys Chem B 108:8364
10. Galoppini E, Rochford J, Chen H et al (2006) J Phys Chem B 110:16159
11. Law M, Greene LE, Johnson JC (2005) Nature Mater 4:455
12. Kubo W, Murakoshi K, Kitamura T et al (1998) Chem Lett p 1241
13. Mohmeyer N, Wang P, Schmidt HW et al (2004) J Mater Chem 14:1905
14. Scully SR, Lloyd MT, Herrera R et al (2004) Synthetic Metals 144:291
15. Kang MG, Kim KM, Ryu KS et al (2004) J Electrochem Soc 151:E257
16. Kim YJ, Kim JH, Kang M et al (2004) Adv Mater 16:1753
17. Longo C, Nogueira AF, De Paoli MA et al (2002) J Phys Chem B 106:5925
18. Tennakone K, Senadeera GKR, Perera VPS et al (1999) Chem Mater 11:2474
19. Haque SA, Park T, Xu C et al (2004) Adv Funct Mater 14:435
20. Komiya R, Han LY, Yamanaka R et al (2004) J Photochem Photobiol A Chem 164:123
21. Kim JH, Kang MS, Kim YJ et al (2004) Chem Commun p 1662
22. Nogueira AF, Longo C, De Paoli MA (2004) Coord Chem Rev 248:1455
23. Kumar R, Sharma AK, Parmar VS et al (2004) Chem Mater 16:4841
24. Suzuki K, Yamaguchi M, Hotta S et al (2004) J Photochem Photobiol A Chem 164:81
25. Krüger J, Bach U, Grätzel M (2000) Adv Mater 12:447
26. Hao Y, Yang M, Li W et al (2000) Sol Energy Mater Sol Cells 60:349
27. Smestad GP, Spiekermann S, Kowalik J et al (2003) Sol Energy Mater Sol Cells 76:85
28. Cervini R, Cheng YB, Simon G (2004) J Phys D Appl Phys 37:13
29. Fukuri N, Saito Y, Kubo W et al (2004) J Electrochem Soc 151:A1745

30. Tan SX, Zhai J, Wan MX et al (2004) J Phys Chem B 108:18693

31. Tennakone K, Kumara GRRA, Kottegoda IRM et al (1998) J Photochem Photobiol A Chem 117:137

32. Tennakone K, Perera VPS, Kottegoda IRM et al (1999) J Phys D Appl Phys 32:374

33. Perera VPS, Pitigala PKDDP, Jayaweera PVV et al (2003) J Phys Chem B 107:13758

34. Kumara GRRA, Konno A, Senadeera GKR et al (2001) Sol Energy Mater Sol Cells 69:195

35. Perera VPS, Pitigala PKDDP, Senevirathne MKI et al (2005) Sol Energy Mater Sol Cells 85:91

36. O′Regan B, Lenzmann F, Muis R et al (2002) Chem Mater 14:5023

37. O′Regan B, Schwartz DT, Zakeeruddin SM et al (2000) Adv Mater 12:1263

38. Bandara J, Weerasinghe H (2005) Sol Energy Mater Sol Cells 85:385

39. Postels B, Kasprzak A, Buergel T et al (2008) J Korean Phys Soc 53:115

40. Wu WB, Jin ZG, Hu GH et al (2007) Electrochim Acta 52:4804

41. Ni Y, Jin Z, Yu K et al (2008) Electrochim Acta 53:6048

42. Pathan HM, Lokhande CD (2004) Bull Mater Sci 27:85

43. Sankapal BR, Goncalves E, Ennaoui A et al (2004) Thin Solid Films 451/452:128

44. Lévy-Clément C, Tena-Zaera R, Ryan MA (2005) Adv Mater 17:1512

45. Sirimanne PM, Jeranko T, Bogdanoff P et al (2003) Semicond Sci Technol 18:708

46. Canava B, Lincot D (2000) J Appl Electrochem 30:711

47. Oekermann T, Boeckler C, Yoshida T et al (2005) J Phys Chem B 109:12560

48. Ni Y, Jin Z, Fu Y (2007) J Am Ceram Soc 90:2966